Computationally Efficient Concurrent Multiscale Framework for the Nonlinear Analysis of Composite Structures

A computationally efficient concurrent multiscale framework for the nonlinear analysis of composite structures

I. Kaleel *, M. Petrolo † and E. Carrera‡
Politecnico di Torino, Torino, Italy, 10129

A.M. Waas§
University of Michigan, 1320 Beal Avenue Ann Arbor, MI 48109-2140

This paper presents a computationally efficient concurrent multiscale platform to undertake the nonlinear analysis of composite structures. The framework exploits refined 1D models developed within the scheme of the Carrera Unified Formulation (CUF), a generalized hierarchical formulation that generates refined structural theories via a variable kinematic description. CUF operates at the macro and microscale, and the macroscale interfaces with a nonlinear micromechanical toolbox. The computational efficiency derives from the ability of the CUF to obtain accurate 3D-like stress fields with a reduced computational cost. The nonlinearity is at the matrix level within the microscale, and its effect scales up to the macroscale through homogenization. The macro tangent matrix adopts a perturbation-based method to have meliorated performances. The numerical results demonstrate that the framework requires some 50% **of the computational time and** 10% **of memory usage of traditional 3D finite elements (FE). Very detailed local effects at the microscale are detectable, and there are no restrictions concerning the complexity of the geometry. The present paper is a companion of a linked work dealing with linear material implementations.**

I. Nomenclature

$\mathbf{C}$	=	material coefficient matrix
$\bar{\mathbf{C}}$	=	homogenized material coefficient matrix
$\mathbf{D}$	=	differential operator matrix
$\mathbf{f}$	=	internal force vector
F_s	=	expansion function of the variation
F_τ	=	expansion function of the variable

*Postdoctoral fellow, MUL^2 Group, Department of Mechanical and Aerospace Engineering, Corso Duca degli Abruzzi 24, 10129, Torino, Italy.
†Assistant Professor, MUL^2 Group, Department of Mechanical and Aerospace Engineering, Corso Duca degli Abruzzi 24, 10129, Torino, Italy.
‡Professor of Aerospace Structures and Aeroelasticity, MUL^2 Group, Department of Mechanical and Aerospace Engineering, Corso Duca degli Abruzzi 24, 10129, Torino, Italy.
§Richard A. Auhll Department Chair of Aerospace Engineering, University of Michigan, 1320 Beal Avenue Ann Arbor, MI 48109-2140

E_1, E_2, E_3	=	Young moduli
G_{12}, G_{13}, G_{23}	=	shear moduli
H	=	strain-hardening modulus
l	=	axial length
$\mathbf{K}$	=	stiffness matrix
N_j	=	shape function of the variation
N_i	=	shape function of the variable
$\mathbf{p}$	=	external force vector
$\mathbf{u}$	=	displacement vector
u_x, u_y, u_z	=	displacement components
V	=	volume
W	=	work
x, y, z	=	reference system axes
δ	=	virtual variation
ϵ	=	strain vector
$\bar{\epsilon}$	=	homogenized strain vector
$\nu_{12}, \nu_{13}, \nu_{23}$	=	Poisson ratios
σ	=	stress vector
$\bar{\sigma}$	=	homogenized stress vector
ϕ	=	yield function
Ω	=	cross-section domain

II. Acronyms

1D	=	One-dimensional
3D	=	Three-dimensional
CUF	=	Carrera's Unified Formulation
CW	=	Component-Wise
DOF	=	number of Degrees Of Freedom
FE	=	Finite Element
Gb	=	Gigabit
GP	=	Gauss Point
LE	=	Lagrange Expansion

MPI = Message Parsing Interface

RVE = Representative Volume Element

III. Introduction

Integrated multiscale modeling of materials and systems to imitate the behavior of the material response at multiple scales is a major enabler for addressing the materials and structures challenges in an effective manner [1]. Although such a modeling technique effectively increases the fidelity of the solution, factors concerning the scalability to practical engineering problems undermine a widespread adoption. Additionally, the significant computational overhead depreciates the overall efficacy of the modeling technique.

Even though continuum-based constitutive models proved to be well-suited for predicting the overall response of structures, modeling localized phenomena such as damage and failure propagation using such approaches remain questionable as such mechanisms depend heavily on the underlying lower-scale features. Micromechanics-based multiscale modeling techniques can help in such cases via computing the effective behavior of the heterogeneous material at the macroscale from the behavior and architecture of the individual constituents [2, 3]. Micromechanics-based multiscale frameworks often consist of the macroscale modeled using FE models and interfaced with a lower microscale with explicit heterogeneous material definitions. Based on the approach adopted at the microscale, a multiscale method can follow a mean-field or full-field approach.

The mean-field approach mostly uses analytical methods such as the concentric cylinder model (CCM) [4], Mori-Tanaka method [5], and generalized self-consistent method (GSCM) [6] to compute the effective response at the microscale. Even though these methods are computationally efficient, the lack of spatially resolved information often restricts their usage in the nonlinear regime. The secant-modulus based approach can extend mean-field theories for the nonlinear analysis but often leads to overestimated responses due to lack of stress concentrations [7]. Zhang and Waas developed an analytical subscale micromechanics model based on two-phase CCM and three-phase GSCM to undertake the nonlinear evolution of matrix constituents within composites and offering distinct computational advantages [8] via the analytical subscale analysis based on a secant method and has been extended by Patel and Waas [9] to make the subscale model more accurate. The method was successful in an integrated multiscale modeling framework for undertaking the progressive failure analysis of laminated fiber-reinforced composites and hybrid 3D textiles [10, 11]. Commercial codes such as DIGIMAT utilize mean-field methods for the multiscale modeling [12].

A class of semi-analytical methods proved to alleviate the limitations of mean-field approaches. Unlike analytical methods, semi-analytical methods offer a spatial resolution of fields with significant computational advantages over fully numerical approaches. The Method of Cells (MOC) [2] and its extensions, including the Generalized Method of Cells (GMC) [13] and High-Fidelity Generalized Method of Cells (HFGMC) [14], are powerful semi-analytical tools

to model the effective behavior of hierarchical materials and structures at the microscale. Such methods can provide the anisotropic response of heterogeneous material via semi-closed-form solutions with a high degree of accuracy. For instance, GMC-based multiscale models are powerful tools for undertaking the progressive failure and damage modeling of composite structures [15–18]. In most cases, the micromechanics toolbox interfaces with a commercial FE solution for the macroscale modeling.

Most commonly adopted fully-numerical approach within the multiscale paradigm are based on FE models applied at both scales, and often referred to as FE^2. Introduced by Feyel for modeling the elasto-visco-plastic analysis of composite structures [19], FE^2 methods is an active area of research [20–23]. Even though the generality of FE facilitates applications to complex problems with highly heterogeneous phases, the high computational cost associated with solving a large set of nonlinear micromechanical boundary value problems at every macro Gauss point impedes the use of the FE^2 method for practical problems such as impact analyses. To an extent, parallel implementations alleviate such a significant computational cost.

Reduced-order modeling is yet another powerful technique to scale down the dimensionality of problems using methods such as the Proper Orthogonal Decomposition (POD) and the Proper Generalized Decomposition (PGD) methods [18, 24–26]. When implemented at the lower scales, such techniques can significantly boost the computational efficiency within a multiscale framework and increase the viability of large-scale problems. Chinesta et al. demonstrated that PGD scales linearly with the dimension of the problem in contrast with the exponentially-growing characteristics exhibited by mesh-based discretization methods [24]. Néron and Ladevèze integrated PGD techniques within the LATIN method for treating multiscale problems and showed significant gains concerning computational costs and storage [25]. Recently, Radermacher et al. presented a new multiscale modeling technique - FEPOD - for the nonlinear analysis by embedding reduced Representative Volume Elements (RVE) based on POD into an FE-based macromechanical simulation [26]. Readers may refer to the review paper by Kanouté et al. for a comprehensive review on recent developments within the multiscale modeling techniques for composites [27].

This paper presents a computationally efficient multiscale framework to model the nonlinear response of composite structures. The concurrent multiscale framework adopts the CUF, a unified framework to obtain any-order structural theories through a variable kinematic formulation [28]. In particular, the proposed methodology makes use of one-dimensional (1D) models having enriched displacement fields over the cross-section. CUF models can provide accurate 3D displacement and stress fields at a reduced computational overhead concerning analysis time and memory usage [29–32]. To date, the computational efficiency of CUF proved to be high for a variety of problems such as progressive failure analysis in composites [29], buckling and post-buckling [30], biomechanics [31], and nonlinear global-local approaches [32].

In the present work, CUF models act at multiple scales to obtain an efficient multiscale framework. The variable kinematic nature of the formulation enables to balance the efficiency and fidelity requirements via exploiting the order

of the formulation as an input of the analysis. Analogously to standard FE^2 methods, 1D CUF models can model the macroscale, i.e., the structural level components such as open-hole specimens and coupons, and the microscale RVE. Explicit FE computations at lower scales are efficient via the CUF Component-Wise (CW) micromechanics approach [33] that can model every constituent retrieving geometrical and material characteristics. In this paper, for comparison purposes, the framework makes use of standard linear brick elements as well. The material nonlinearity acts at the microscale and then upscales back to the macroscale through the homogenization. A perturbation method enables an efficient numerical calculation of the tangent matrix [34] to improve the convergence behavior at the macroscale. Parallelization of the framework uses a hybrid OpenMP-MPI approach.

The paper structure is the following: Section IV describes in detail various aspects of the multiscale framework. Three sets of numerical cases are discussed in Section IV. Concluding remarks are drawn in Section VI.

IV. Nonlinear concurrent multiscale framework

A. Nonlinear CUF

According to the CUF, the 3D displacement field $\mathbf{u}(x, y, z)$ makes use of generic expansions of the primary unknowns. In the 1D case, the displacement becomes

$$\mathbf{u}(x, y, z) = F_\tau(x, z)\mathbf{u}_\tau(y), \qquad \tau = 1, 2, ..., M \tag{1}$$

where $F_\tau(x, z)$ are the expansion functions acting at the cross-section level, x-z plane, and have M terms. $\mathbf{u}_\tau(y)$ is the generalized displacement field along the beam axis. Various basis functions can define F_τ and this choice determines the class and order of the 1D CUF models. The present work uses Lagrange polynomials as expansion functions, referred to as LE models, and characterized by having only pure displacements as primary unknowns. More details on LE models are in Carrera and Petrolo [35].

Via FE along with the y-axis, the displacement field becomes

$$\mathbf{u}(x, y, z) = N_i(y)F_\tau(x, z)u_{\tau i} \qquad \tau = 1, 2, ..., M; \quad i = 1, 2, ..., p + 1 \tag{2}$$

where N_i is the shape function of order p and $u_{\tau i}$ is the nodal unknown vector. Via the principal of virtual displacements,

$$\delta W_{int} - \delta W_{ext} = 0 \tag{3}$$

where W_{int} and W_{ext} are the internal work and work due to external loading respectively and δ denotes the virtual variation. In the case of nonlinear analysis, the governing equations become a system of nonlinear algebraic equations,

$$K_s^{ij\tau s} u_{\tau i} - p_{\tau i} = 0 \tag{4}$$

where $\mathbf{k}_s^{ij\tau s}$ and $p_{\tau i}$ are the fundamental nucleus of the secant stiffness matrix and of external loading vector, respectively. The derivation and implementation aspects for formulating such nuclei are in Carrera et al. [28]. Via Eq. 4, the global assembled FE matrices for a generic higher-order 1D model by expanding the nuclei using indices $\tau, s = 1, 2, ..., M$ and $i, j = 1, 2, ..., p + 1$,

$$\mathbf{K}_S \mathbf{u} - \mathbf{p} = 0 \tag{5}$$

where $\mathbf{K}^s$, $\mathbf{u}$ and $\mathbf{p}$ are the global assembled FE arrays. By adopting the Newton-Raphson method, the incremental linearized of Eq. 5 becomes

$$\mathbf{K}_T(\mathbf{u})\Delta\mathbf{u} = \lambda\mathbf{p} - \mathbf{f}_{int}(\mathbf{u}) \tag{6}$$

where $\mathbf{K}_T$ is the global tangent stiffness matrix, λ is the load scaling parameter and $\mathbf{f}_{int}$ is the global internal force vector. Since the current work restricts to the physical nonlinearity, the tangent fundamental nucleus is [36]:

$$\mathbf{k}_{ij\tau s}^{tan} = \int_l \int_\Omega \mathbf{B}^T (N_i(y) F_\tau(x,z))\, \mathbf{C}_{tan}\, \mathbf{B}(N_j(y) F_s(x,z)) dl\, d\Omega \tag{7}$$

where $\mathbf{B}$ is a differential operator and $\mathbf{C}_{tan}$ is the tangent material matrix. Within the multiscale framework, the tangent material matrix at the microscale makes use of the constitutive modeling of the material behavior, e.g., the elastoplastic tangent matrix. At the macroscale, the lack of analytically derivable constitutive equations compels to formulate the material tangent numerically. A perturbation method provides such a numerical scheme [34], see Section IV.D.

B. Constitutive models

In this work, the nonlinear response of the structure stems from the inelastic behavior exhibited by the individual constituents at the micro level, in particular, the nonlinearity originates within the matrix. On the other hand, fiber is linear elastic. The inelastic model for matrix accounts for plasticity to simulate the shear-driven nonlinear behavior [37, 38].

Based on the incremental theory of plasticity, the infinitesimal strain increment in matrix, $d\boldsymbol{\epsilon}_m$, have and elastic, $d\boldsymbol{\epsilon}_m^e$,

and plastic, $d\boldsymbol{\epsilon}_m^p$, strain component,

$$d\boldsymbol{\epsilon}^m = d\boldsymbol{\epsilon}_m^e + d\boldsymbol{\epsilon}_m^p \tag{8}$$

Assuming the von Mises plasticity potential, the yield function reads

$$\phi = J_2(\boldsymbol{\sigma}) - \sigma_m^y \tag{9}$$

where $J_2(\boldsymbol{\sigma})$ is the von Mises plastic potential and σ_m^y is the yield stress of the matrix [39]. The incremental stress, $\boldsymbol{\sigma}$, is related to $d\boldsymbol{\epsilon}_m^p$ through following associative flow rule :

$$d\epsilon_{ij}^p = d\lambda \frac{\partial \phi}{\partial \sigma_{ij}} \tag{10}$$

where $d\lambda$ is the proportionality factor expressed as:

$$d\lambda = \frac{3}{2}\frac{d\boldsymbol{\epsilon}^p}{\boldsymbol{\sigma}} = \frac{3}{2}\frac{1}{H^m}\frac{d\boldsymbol{\sigma}}{\boldsymbol{\sigma}} \tag{11}$$

where H^m is the strain-hardening modulus from experimental data. More details on the numerical aspects regarding the implementation of plasticity models within CUF, including the formulation for of the elastoplastic tangent matrix C_{ep}^m, are in Carrera et al. for [36].

C. Micro model: CW micromechanical framework

As in Fig. 1, the CUF micromechanics framework models the RVE as beams using the CW approach [33]. The RVE has its cross-section discretized in some Lagrange elements. The cross-section domain is $x_2 - x_3$ and extends along the beam direction, x_1. The local refinement in the RVE is achievable through the discretization of the RVE using multiple L9 elements in the cross-section, in which L9 indicates a nine-node element. The beam element may have two, three or four nodes, namely, B2, B3 or B4. Periodic boundary conditions maintain the compatibility of displacement and stress along the faces of the RVE as in Kaleel et al. [33]. The homogenized response of the RVE uses the volume averaging of the macrostate variables, $\bar{\mathbb{H}}$, from the local microstate variables, $\mathbb{H}$, computed at every Gauss point of the RVE,

$$\bar{\mathbb{H}} = \frac{1}{V}\int_V \mathbb{H} dV \tag{12}$$

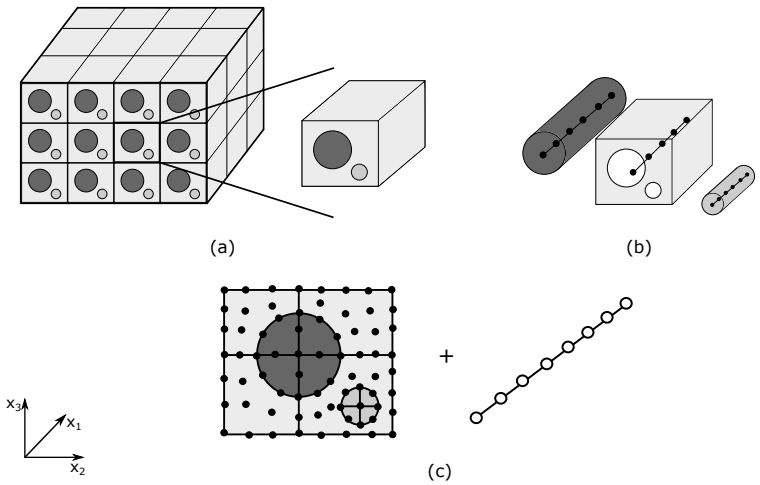

Fig. 1 An illustration of the CW modeling of a composite microstructure with arbitrary constituents: (a) a triply periodic composite microstructure with three different phases, (b) a triply periodic RVE with individual components modeled as separate components and (c) assembled cross-section with Lagrange elements along with the beam for the RVE

D. Numerical computation of consistent macroscopic tangent matrix

The efficiency and convergence behavior of a multiscale iterative scheme hinges on accurate computation of the macroscopic tangent matrix, which must be consistent with the macroscopic stress evolution. The lack of explicit macroscale constitutive formulations necessitates the extraction of macroscopic stress and material tangent matrix in an ensemble-averaged sense. The numerical tangent matrix computation within a multilevel FE framework originated in Kouznetsova et al. [40], via a fourth-order consistent macroscopic tangent tensor condensing the micro FE tangent matrix. The procedure involves the computation of the Schur complement for the matrix inversion, which could be memory expensive for large micro models. In this work, the computation of the macroscopic tangent matrix is numerical via a perturbation technique based on the forward difference approximation developed by Miehe and Koch [41]. Such a numerical scheme has proved successful in a wide range of nonlinear multiscale problems [34, 42, 43].

The macroscopic material tangent matrix exploits the numerical linearization around the current macroscopic loading and stems from applying six infinitesimally small perturbation strains $\delta\boldsymbol{\epsilon}$ on the current equilibrium strain field,

$$\delta\boldsymbol{\sigma} = \mathbb{C}_{\delta\boldsymbol{\epsilon}}\delta\boldsymbol{\epsilon} \tag{13}$$

where $\delta\boldsymbol{\sigma}$ is the perturbed stress due to applied perturbed strain $\delta\boldsymbol{\epsilon}$. The perturbation value depends on the machine precision, as too small values may lead to numerical problems and error would accumulate in the case of large values [34]. In this work, the perturbation value $||\delta\boldsymbol{\epsilon}||$ is set as 10^{-6}, which yielded sufficiently accurate results. During the perturbation step, the internal variables $\mathbb{H}$ must be able to evolve to obtain a consistent numerical tangent matrix [34]. Therefore, the perturbation takes place by adding the perturbed strain to the current macro strain. The perturbed stress

$\delta\bar{\boldsymbol{\sigma}}$ increment is

$$\delta\bar{\boldsymbol{\sigma}}^{n+1} = \bar{\boldsymbol{\sigma}}(\boldsymbol{\epsilon}^{n+1} + \delta\boldsymbol{\epsilon}, \mathbb{H}^{n+1} + \delta\mathbb{H}) - \bar{\boldsymbol{\sigma}}(\boldsymbol{\epsilon}^{n+1}, \mathbb{H}^{n+1}) \tag{14}$$

Each column of the numerical tangent matrix $\mathbb{C}_{\delta\boldsymbol{\epsilon}}$ stems from solving six nonlinear microscopic systems.

E. Concurrent implementation and parallelization

The generality within the CUF framework facilitates the usage of the same implementation scheme at multiple scales. Additionally, the variable kinematic nature of the framework aids in integrating various classes of FE efficiently. The macroscale interfaces with the microscale by updating the macro Gauss points. Such an update derives from the current incremental macro strain passed to the microscale as an input. The micro framework computes the updated macro tangent matrix, macro stress and solution variables, and sends it back to update the macro Gauss points. Due to the iterative nature of the framework, the solution variables of every Gauss point within the micro RVE associated with a macro Gauss point need storage, leading to an exponential increase in the memory usage as the size of the numerical problem grows. To alleviate such a problem, the current framework stores the solution variables for micro RVE only when it enters the nonlinear regime.

Further efficiency stems from the use of a hybrid MPI-OpenMP based parallelization strategy [44]. MPI-based constructs parallelize the global level operations such as updating solution variables at macro Gauss points and the global stiffness assemblage. OpenMP commands act at the local level operations, such as the macro tangent computation, by parallelizing the six nonlinear solutions. Within the multiscale framework, since the majority of the analysis time addresses the solving of the micromechanical nonlinear problem at every macro Gauss point, the parallelization strategy adopted above yields a near-ideal speedup as depicted in Fig. 2.

V. Numerical results

This section presents three sets of numerical cases. The validation and assessment of the robustness of the framework is the aim of the first case dealing with a multilayered structure under pure shear loading conditions. The second set investigates the nonlinearity exhibited by off-axis laminates including comparisons against experimental results. The last case shows the nonlinear response of an open-hole specimen.

The present framework can handle standard eight-node brick FE, commonly used in literature for FE^2 framework based multiscale analyses. Depending on the kind of FE used in the two scales, the numerical results stem from various multiscale models, as enlisted in Table 1.

A. Nonlinear shear response of multilayered composites

The present numerical case deals with a multilayered structure under pure shear loading conditions. The problem definition derives from the work of Tikarrouchine et al. [21]. The microscale model has a periodic stack of two

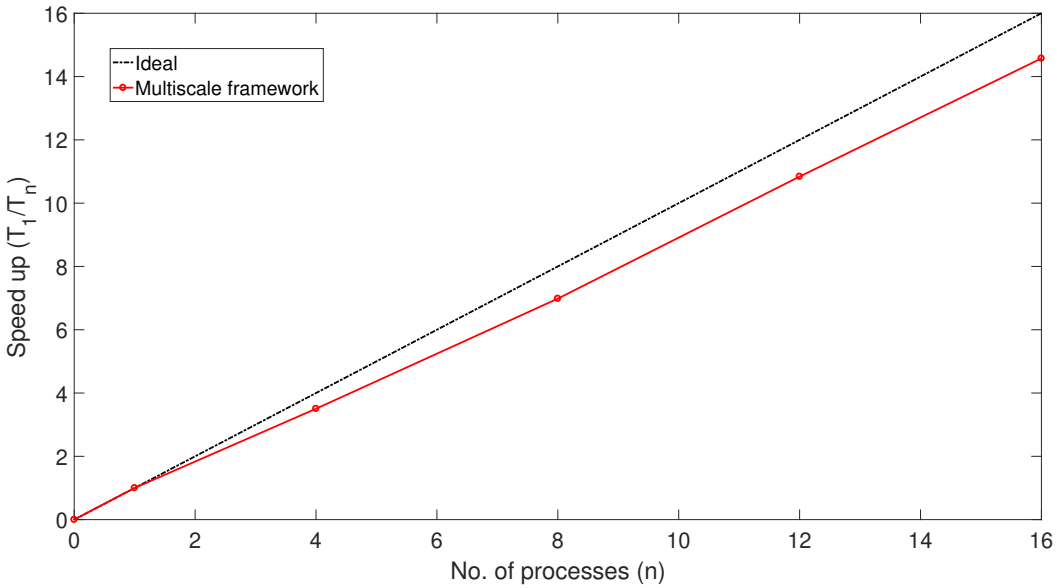

Fig. 2 Speed up obtained in the parallel version of nonlinear multiscale framework for the second numerical case

Table 1 Nomenclature for various models used in multiscale analyses

Model name	Macroscale	Microscale
1D-1D	CUF beam element	CUF beam element
3D-1D	Standard linear 3D brick element	CUF beam element
3D-3D	Standard linear 3D brick element	Standard linear 3D brick element

Table 2 Material properties for the two-layered RVE under pure shear loading conditions

	Volume fraction [-]	Young modulus [GPa]	Poisson ratio [-]	Yield Stress [MPa]
Elastic phase	0.5	6.0	0.2	-
Elastoplastic phase	0.5	2.0	0.3	10.0

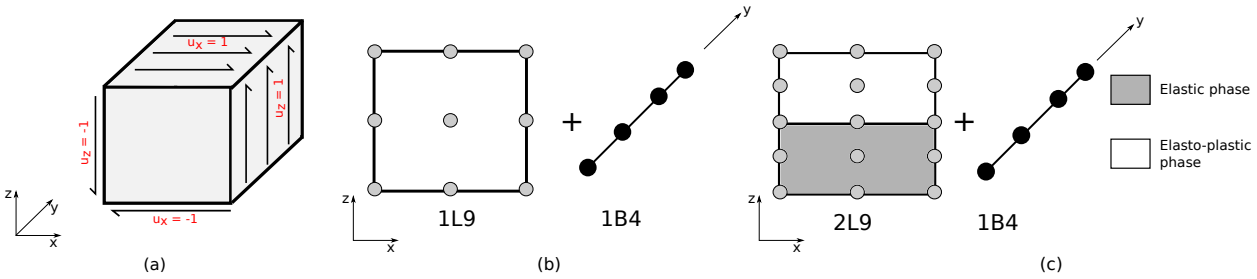

Fig. 3 Model information of the two-layered RVE under pure shear loading conditions: (a) Boundary conditions for macro model, (b) Cross-section and beam modeling of macro model and (c) Cross-section and beam modeling for micro model

composite layers with a volume fraction of 0.5 each. As in Fig. 3(c), the first layer has as an elastic material whereas the second layer exhibits an elastoplastic response with material parameters tabulated in Table 2. Figure 4 depicts the plastic response of the elastoplastic phase, based on the power-law hardening function. The boundary conditions of the macrostructure correspond to a pure shear loading case, see Fig. 3(a). The macrostructure is a cube modeled using 1 L9 along the cross-section and 1 B4 along the beam axis, as depicted in Fig. 3(b). The dimensions of the cube are unitary. Since the boundary conditions imposed on the macro model yield pure shear loadings, i.e., all strain components except ϵ_{23} are zero, the overall response of the macrostructure must be identical to the micromechanical analysis of the RVE with an imposed non-zero shear strain ϵ_{23}.

Figure 5 shows the overall macro response along with results from the CUF-micromechanical analysis, semi-analytical solutions and the reference FE^2 solution from Tikarrouchine et al. [21].

The assessment of the convergence behavior of the framework is the aim of another analysis having a total strain of the 5% applied in one large increment. Similarly to the study undertaken by Haj-Ali and Aboudi in [17], this study aims at evaluating the robustness of the framework to handle severe nonlinearities. Figure 6 shows the convergence behavior regarding the norm of the residual vector of the 1D-1D model versus the CUF micro model, where 1D-1D (Global) refers to the multiscale global convergence behavior of the macro 1D model and 1D-1D (Local) refers to the convergence behavior exhibited at the local micromodel interfaced to one of the Gauss points of the macro model. Results suggest the following:

1) From Fig. 5, it is evident that the overall macro response of 1D-1D matches well with CUF micromechanics and reference solutions.

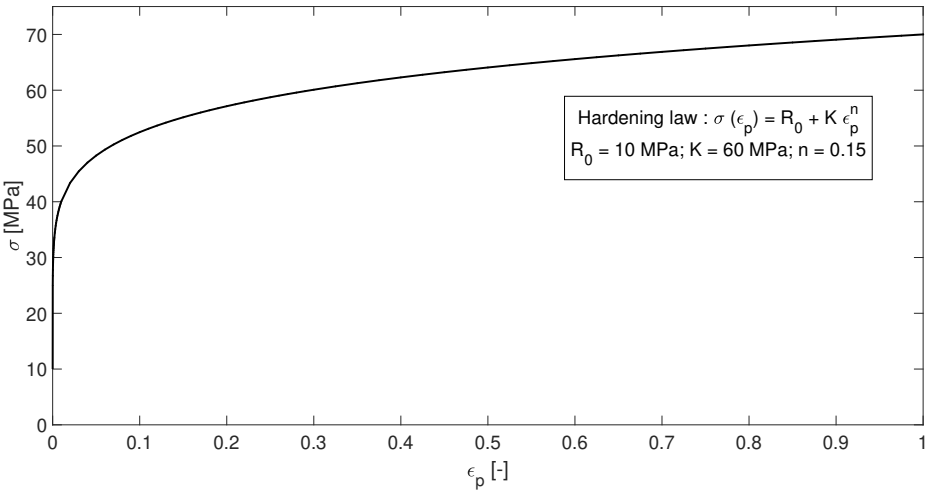

Fig. 4 Plastic response of the elastoplastic phase for the two-layered RVE under pure shear loading conditions

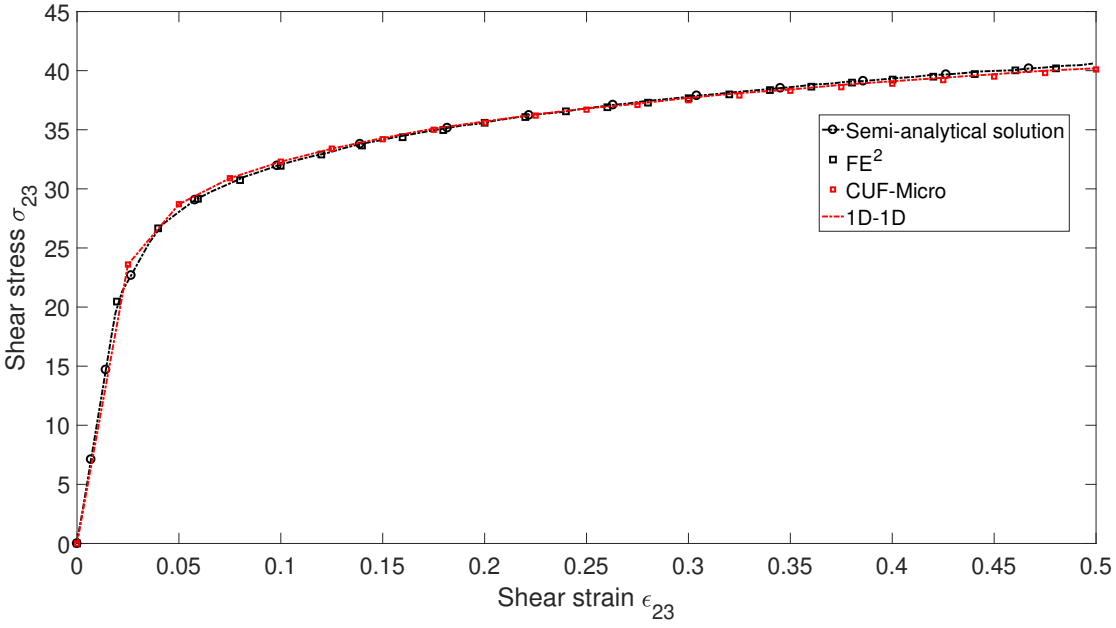

Fig. 5 Comparison of the overall macro response of the two-layered RVE under pure shear loading conditions against semi-analytical solutions and the FE^2 approach

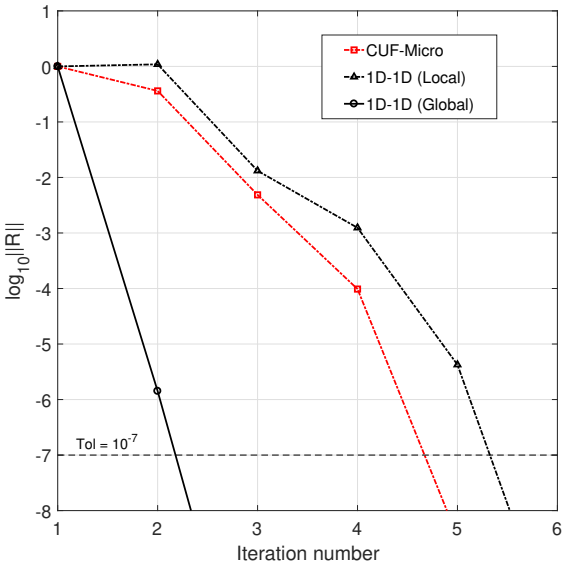

Fig. 6 Comparison of convergence between 1D-1D model and CUF-micro model

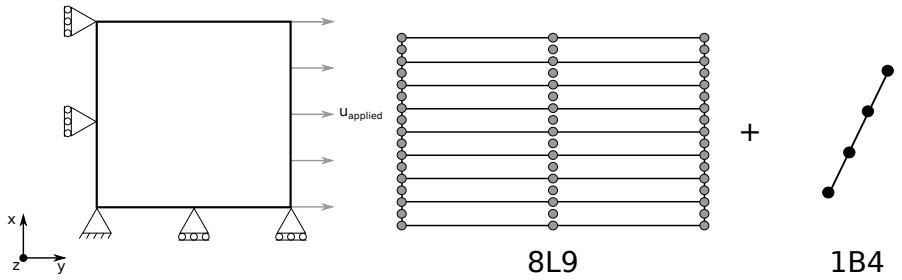

(a) Boundary conditions

(b) Macro model of the unnotched laminate under uniaxial tension

Fig. 7 1D-1D macro model

2) The convergence behavior of CUF micro and 1D-1D (Local) matches the findings of Haj-Ali and Aboudi in [17]. On the other hand, the multiscale framework, i.e., 1D-1D (Global), exhibits a superior convergence, see Fig. 6.

B. Unnotched plate under uniaxial tension

O'Higgins et al. conducted experimental and numerical investigations on the nonlinear response of off-axis glass fiber-reinforced composite laminates under tension [45, 46]. The emergence of permanent strains in specimens during cyclic loading revealed the plastic-like behavior of laminates. The authors also developed a Continuum Damage Mechanics (CDM) plasticity model for the lamina for undertaking numerical analyses of off-axis laminates under tension [46], which shall serve as a reference solution for the following study.

In this paper, the inelastic deformation phenomenon stems from modeling the matrix plastic deformation at the microscale. The numerical results deal with three stacking sequences, namely, $[10]_{2s}$, $[55]_{2s}$ and $[67.5]_{2s}$. The multiscale models adopted are the following:

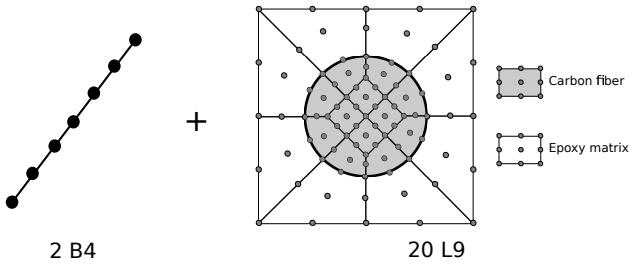

Fig. 8 Micro model for the 1D-1D multiscale of the unnotched laminate under uniaxial tension

Table 3 Micro model information for the unnotched laminate under uniaxial tension

Micromodel	Information	DOF	GP	Analysis time per increment [s]	
				Without tangent	With tangent
1D-1D	CUF beam element - 20 L9 cross-section elements with 2 B4 beam elements	1,869	1,440	0.45	2.90
3D-3D	1656 linear brick elements (2 elements per layer)	6,405	13,248	0.75	5.24

DOF: Degrees of freedom. GP: Gauss points.

(a) 1D-1D: Microscale and macroscale models have 1 B4 element with 1 L9 element per layer, see Fig. 7(b). The total number of Gauss points in the macrostructure is 288.

(b) 3D-3D: Analogously to the traditional FE^2 method and similarly to the modeling technique undertaken by O'Higgins at al. [46], both scales use two linear 3D brick elements per layer. the total number of Gauss points in the macrostructure is 1152.

The thickness of each layer is 0.125 mm and Fig. 7(a) shows the boundary conditions of the macrostructure having unitary length and width.

As depicted in Fig. 8, the micro structure model is a square-packed RVE. In the 1D-1D case, the micro model consists of 20 L9 along the cross-section and 2 B4 along the beam with 1869 degrees of freedom (DOF). In the 3D-3D case, the mesh adopted derived from Kaleel et al. [33] and consisted of 1656 brick elements amounting to 5796 DOF. The model information for the microscale models are in Table 3 along with analysis time with and without macro tangent material matrix computation. The fiber is transversely isotropic linear elastic and the von Mises plasticity models the inelastic deformation in matrix constituents. The transverse and shear response of the RVE derives from calibration to

Table 4 Elastic properties of the RVE for the unnotched laminate under uniaxial tension

	E_1 (GPa)	E_2 (GPa)	G_{12} (GPa)	G_{23} (GPa)	ν_{12} (-)
HTA Fiber	223.0	23.0	32.0	7.0	0.28
MY750 matrix	4.3	4.3	1.7	1.7	0.27

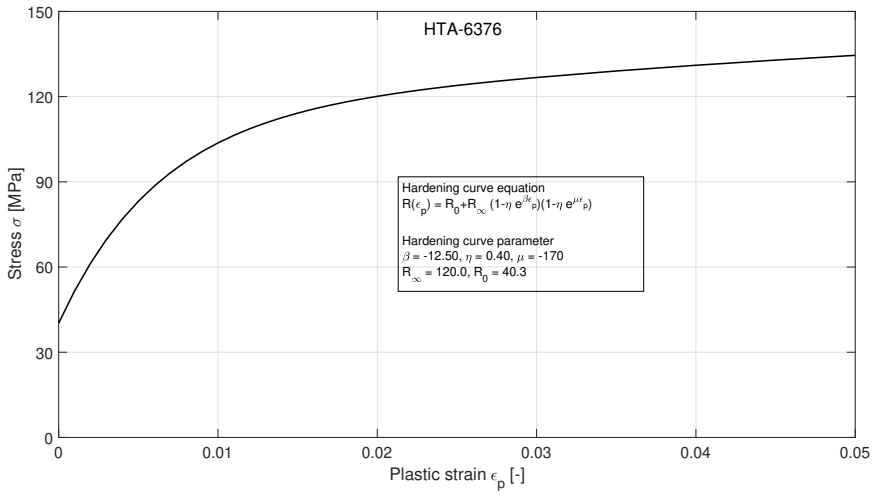

Fig. 9 Calibrated hardening curve used for the RVE model of the unnotched laminate under uniaxial tension

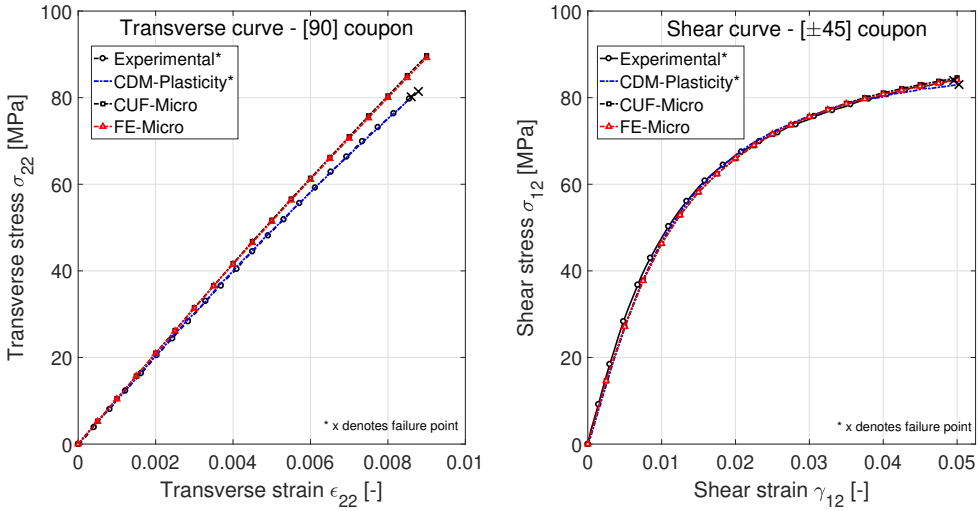

Fig. 10 Comparison of calibrated 1D CUF-Micro and 3D FE-Micro model against experimental [45] and CDM plasticity model [46] for transverse and shear response of the RVE

experimental data available for [90] and [±45] coupons [45], see Table 4. The hardening curve of the matrix plasticity model makes use of a four parameter model [47] as shown in Fig. 9.

Figure 10 presents the overall response of 1D, referred to as CUF-Micro, and 3D, referred to as FE-Micro, micro models under transverse and shear loadings with comparison against experimental [45] and literature solutions [46]. Figure 11 shows the accumulated plastic strain in calibrated RVE models at an applied shear strain $\gamma_{12} = 0.05$.

The calibrated microscale RVE models interface with the macro models for the three different laminate systems. Figure 12 compares the tensile stress versus strain with comparison against experimental [45] and CDM plasticity model results [46]. It is important to emphasis that both the reference results include the final failure point whereas the current simulation restricted to only modeling the nonlinear behavior. Table 5 enlists the total time taken for the analysis and the

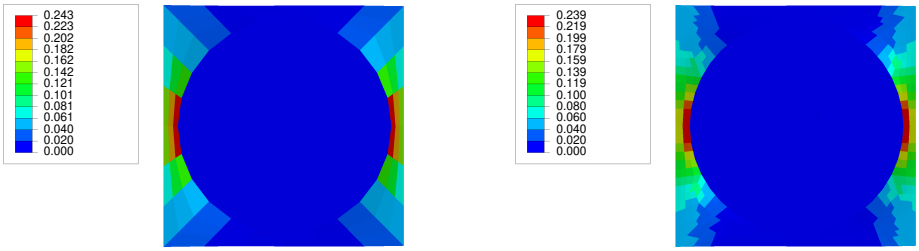

(a) 1D CUF-micro (b) 3D FEM-micro

Fig. 11 Accumulated inelastic strain in calibrated RVE at an applied shear strain $\gamma_{12} = 0.05$

Table 5 Numerical results for the unnotched laminates under uniaxial tension

Laminates	$[10]_{2s}$		$[55]_{2s}$		$[67.5]_{2s}$		Average	
Model	1D-1D	3D-3D	1D-1D	3D-3D	1D-1D	3D-3D	1D-1D	3D-3D
Total analysis time (hh:mm)	0:47	2:32	0:50	2:12	0:39	2:20	**0:46**	**2:22**
Average memory usage per core (Gb)	1.52	28.1	1.51	28.0	1.51	28.1	**1.51**	**28.1**

memory usage for different multiscale models. The numerical results suggest that

1) Figure 11 shows that 1D micro models exhibit similar accumulated inelastic strain field in comparison to 3D micro models under shear loading.
2) In comparison to experimental and reference results, both multiscale approaches capture varying degree of nonlinearity exhibited by different laminates with acceptable accuracy, see Fig. 12.
3) Table 4 shows that 3D micro models require twice the time to undertake a single micro RVE analysis in comparison to 1D models. The speed-up obtained affects the overall analysis time for the multiscale analysis with 1D-1D requiring only 46 minutes whereas 3D-3D needs 2 hours and 22 minutes on average, see Table 5.
4) Significant differences characterize the memory usage of the multiscale models, see Table 5. Such a difference stems from the large variation in the required number of Gauss points in the microscale for both models. In fact, 1D uses 1,440 Gauss points whereas 3D requires 13,248 Gauss points. On average, 1D-1D models are 18 times more memory-efficient than the respective 3D-3D models.

C. Open-hole specimen under tension

The last numerical case focuses on an open-hole specimen under tension, as illustrated in Fig. 13. The specimen has an imposed displacement of 0.5625 mm applied in 20 incremental steps. The three multiscale models have the same micro model but differ concerning the macro models,

(a) 1D-1D: The cross-section of the macro model has 37 L9 with each layer modeled with B2 beam elements.
(b) 3D-1D Coarse: The macro model has 792 3D linear brick elements, one element per layer.

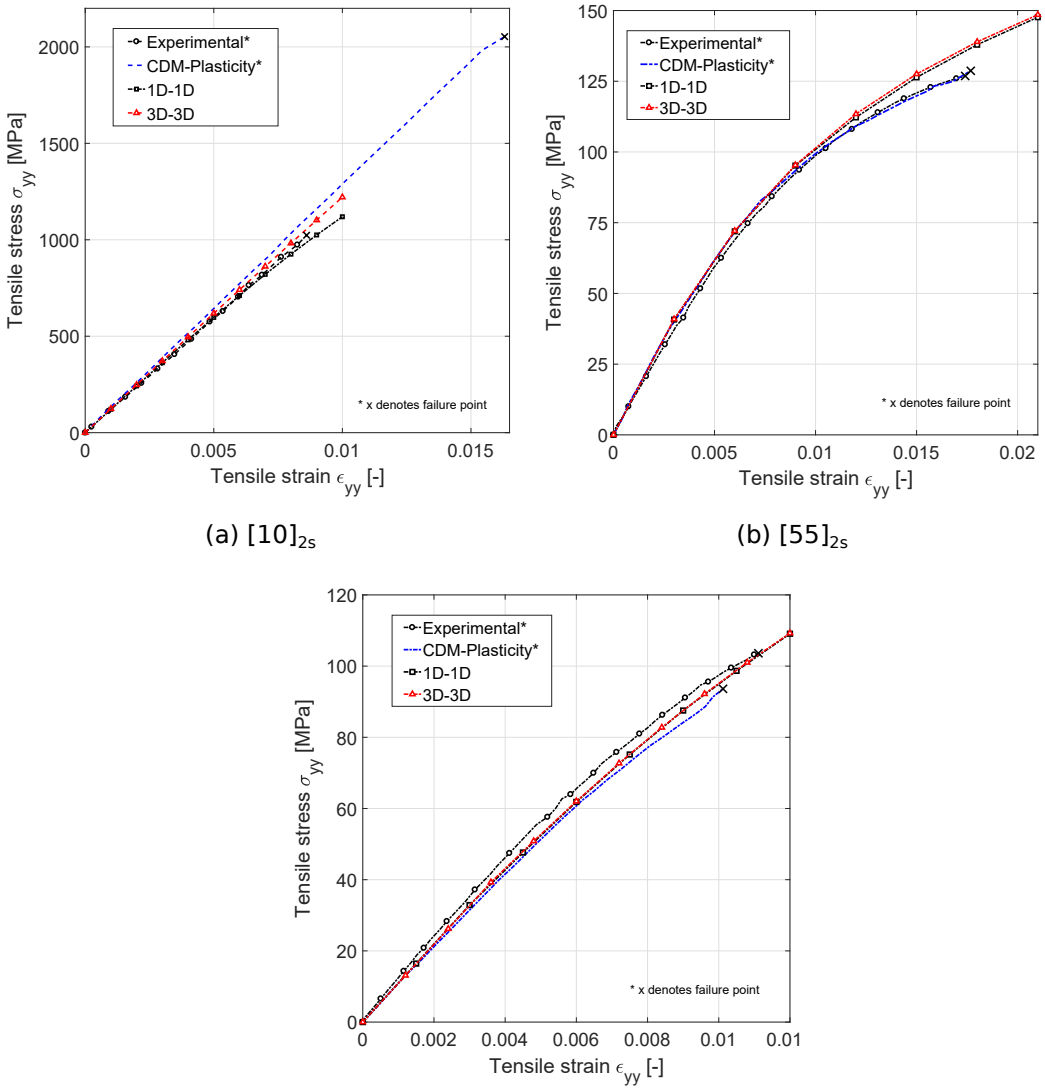

Fig. 12 Comparison of multiscale model predictions against experimental data [45] and CDM plasticity model [46] for unnotched laminates under uniaxial tension

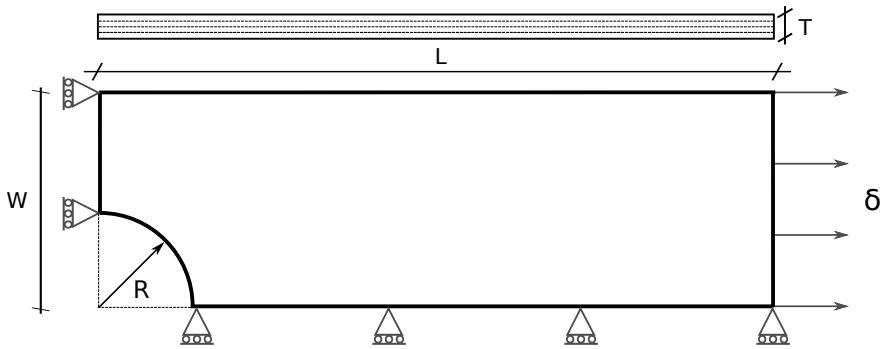

Fig. 13 Geometry and boundary condition for the open-hole specimen under tension

Table 6 Computational information for the open-hole specimen models

Model	Information	DOF	GP	Total analysis time [hh:mm:ss]	Memory requirement [Gb]
1D-1D	37 L9 cross-section element with 4 B2 beams	2,655	2,664	01:53:38	2.02
3D-1D Coarse	792 3D brick elements with one element per layer	3,450	6,336	05:27:12	7.28
3D-1D Refined	1088 brick elements with one element per layer.	4,650	8,704	08:24:37	8.75

(c) 3D-1D Refined: The mesh density is increased around the hole region, thereby raising the total number of 3D brick element used to model the specimen to 1088. One element is used to represent each layer.

The micro model consists of a fiber-reinforced composite system with an elastoplastic matrix. Fiber is linear isotropic material with a Young modulus $E = 414\ GPa$, Poisson ratio $\nu = 0.15$, and has a volume fraction of 0.6. The material properties of the matrix are in Fig. 14 with the yield stress and post-yield hardening curve. Figure 15 shows the mesh configurations for the different multiscale models. Due to the high-stress gradient within the zone around the hole, the material nonlinearity in the micro model is active only in the integrations points within the shaded region in Fig. 15. Table 6 enlists the model information along with analysis time and memory requirements.

Figure 16 depicts the remote stress-strain response via the three multiscale models. The remote stress is the reaction force at the applied displacement end divided by its area. The ratio between the applied displacement and the length of the specimen is the remote strain. Figure 17 shows the accumulated inelastic strain via various multiscale models including the spatial resolution of the equivalent inelastic strain at the microscale. Figure 18 presents the von Mises stress distribution within the matrix constituent of the micro RVE for various multiscale models. Stress contour plots for

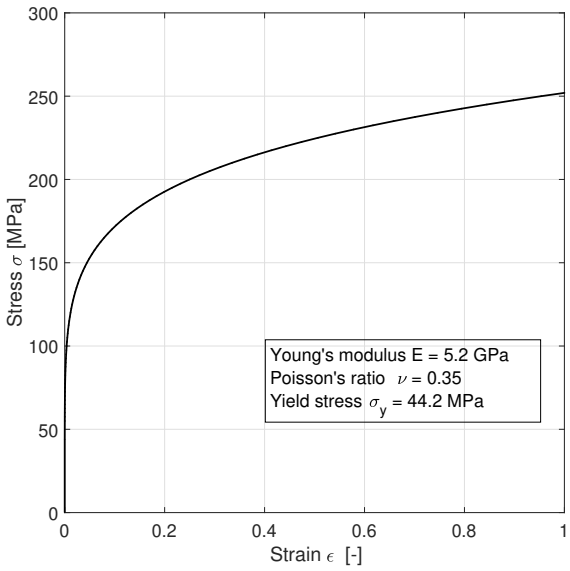

Fig. 14 Material properties for the inelastic matrix for the micro model of the open-hole specimen under tension

individual plies in the macro model are in Fig. 19. Figure 20 shows the convergence behavior of the multiscale models by comparing the number of iterations required at each loading increment. The numerical results suggest that

1) From Fig. 16, 1D-1D and 3D-1D refined exhibit similar remote stress-strain responses.
2) The contour plots for accumulated inelastic strain at both scales illustrate the superior capability of the 1D-1D model to capture the nonlinear behavior across scales, see Fig. 16. Figure 18 further emphasizes the capabilities of the framework by comparing the von Mises stress field at the microscale.
3) According to Table 6, 1D-1D exhibits multifold efficiency concerning the analysis time.
4) Even though all multiscale models interface with the same micro 1D model, 1D-1D requires only 2,664 macro Gauss points whereas 3D-1D coarse and 3D-1D refined need 6,336 and 8,704 Gauss points, respectively. Therefore, the total memory requirement for 1D-1D is 2.02 Gb whereas 3D-1D coarse and 3D-1D refined need, 7.28 Gb and 8.75 Gb, respectively.
5) Figure 20 shows that the present framework exhibits good convergence behavior via the numerical computation of the full tangent matrix of the macro model through the perturbation method. For the current analysis, the framework required on average three iterations per load increment.

VI. Conclusions

This paper presents a computationally efficient concurrent multiscale framework for modeling the nonlinear behavior of multilayered structures. Built within the scheme of CUF - a unified framework to generate any-order structural theories through a variable kinematic formulation -, the present approach exploits CUF models at the macroscale to model

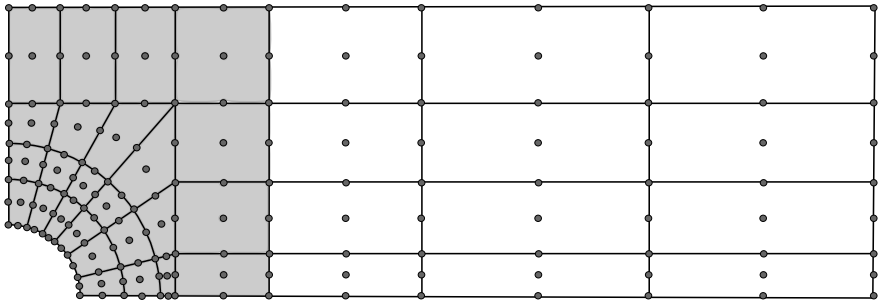

(a) 1D macro model with 37 L9 cross-section elements and 1 B2 per layer

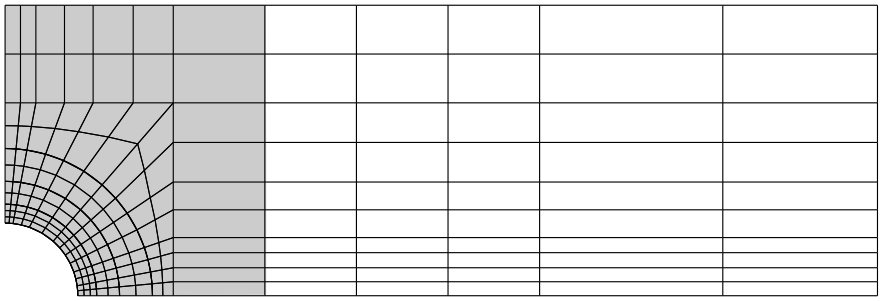

(b) 3D coarse macro model with 792 3D brick elements

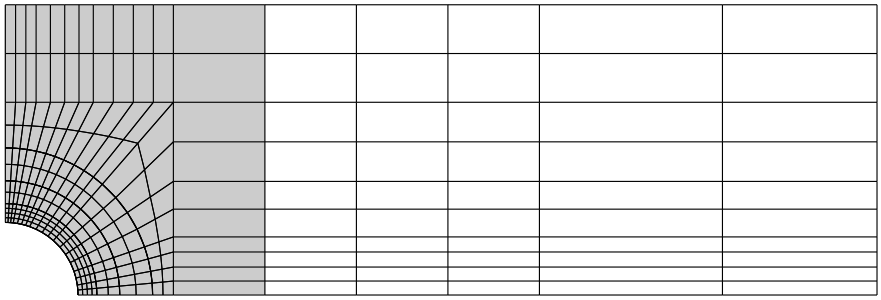

(c) 3D Refined macro model with 1088 3D brick elements

Fig. 15 Mesh configurations for various multiscale models for the open-hole specimen under tension

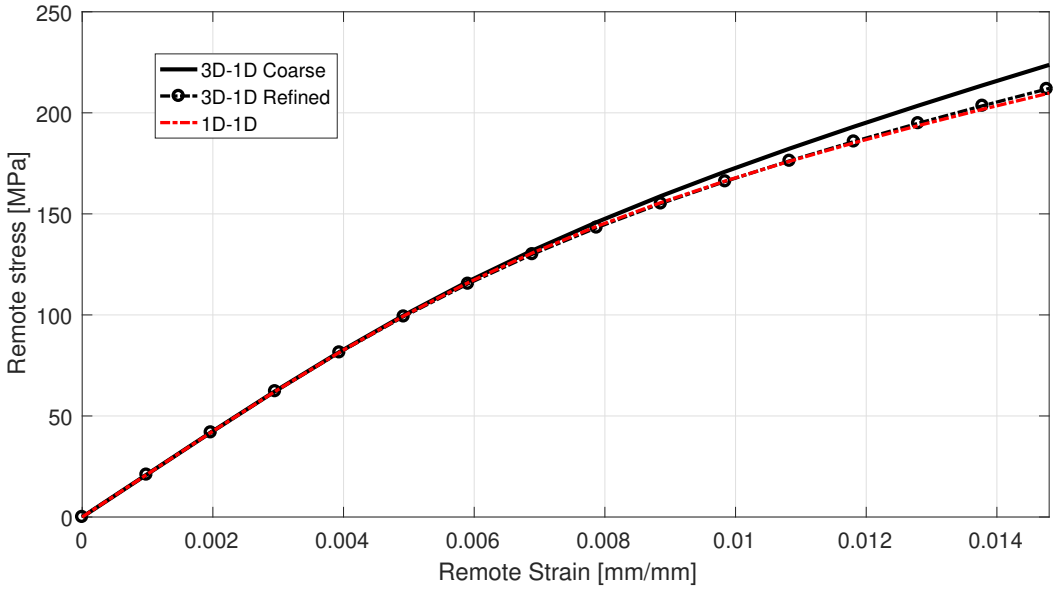

Fig. 16 Remote stress-strain curve for open-hole specimen under tension

the structural level components, e.g, open-hole specimens plates, interfaced with an efficient CUF micromechanics toolbox. The nonlinearity is at the constituent level within the microscale and the effect scales up to the macrostructure via homogenization. A perturbation-based numerical homogenization scheme leads to the macro tangent matrix and enables a numerically efficient framework. According to the numerical results,

1) The proposed framework exhibits multifold enhancements of efficiency concerning the analysis time and memory usage as compared to traditional multiscale implementations based on 3D FE.
2) The accuracy of the solution is high and comparable to 3D FE. In particular, detailed local effects at the microscale are obtainable.
3) The capability of using the same 1D formulation at every scale independently of the complexity of the material system and geometry makes the present methodology appealing as a way to reduce the computational overhead of multiscale frameworks.

Future work shall include integrating damage models within the microscale to model complete failure of the structure. Damage models often exhibit convergence issues, dictating smaller load increments, may affect the computational efficiency and needs to be further studied. Scaling the framework to computationally intensive problems such as impact is also a future task. A key issue for an explicit dynamic analysis is the computational effectiveness. The present model can be an alternative to standard FEM-based micromechanics due to superior efficiency. Also, an explicit numerical integration does not require macro tangent matrix computations with further enhancements in the efficiency.

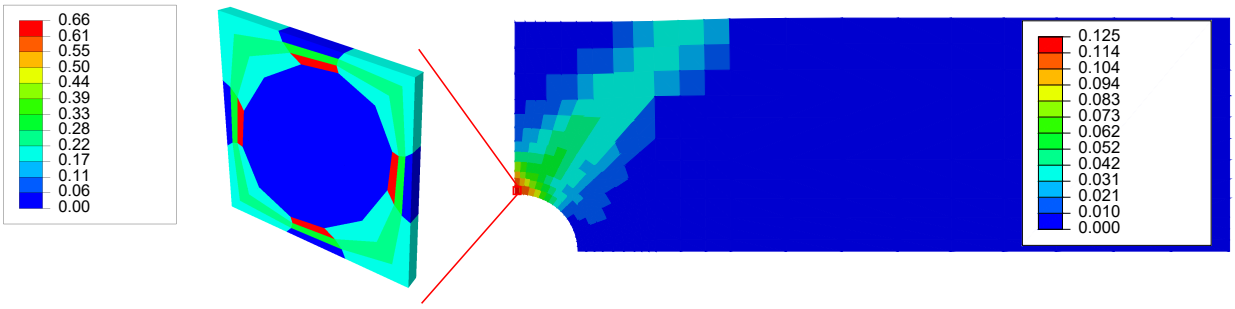

(a) 1D-1D

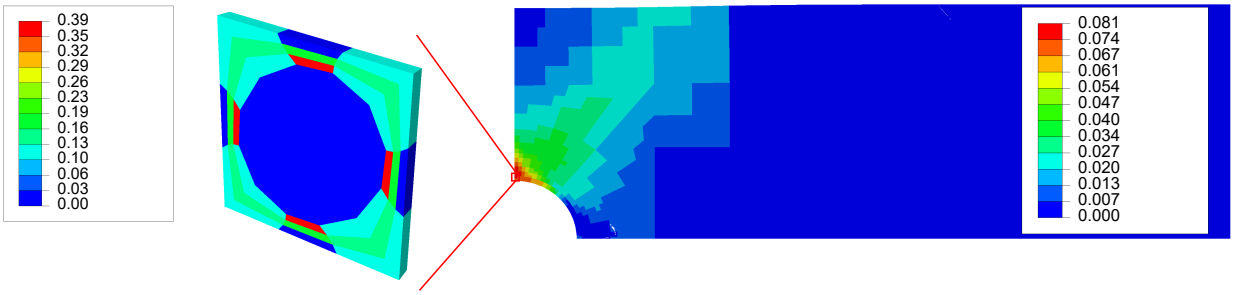

(b) 3D-1D Coarse

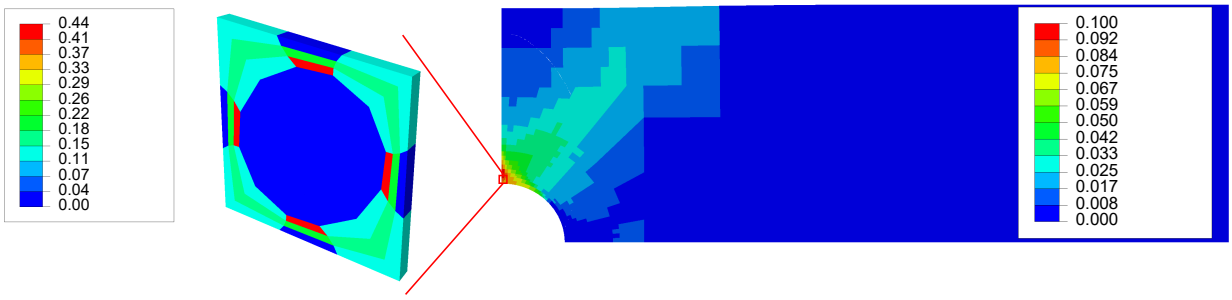

(c) 3D-1D Refined

Fig. 17 Comparison of accumulated inelastic strain at multiple scales via various multiscale models for the open-hole specimen under tension at an applied displacement loading of 0.5625 mm

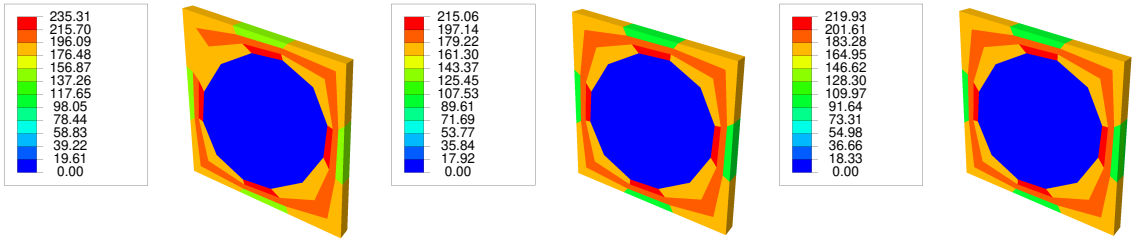

(a) 1D-1D (b) 3D-1D Coarse (c) 3D-1D Refined

Fig. 18 Comparison of von Mises stress resolution within matrix constituents of the RVE via various multiscale models for the open-hole specimen under tension at an applied displacement loading of 0.5625 mm. Refer to Fig. 17 for the RVE posistion

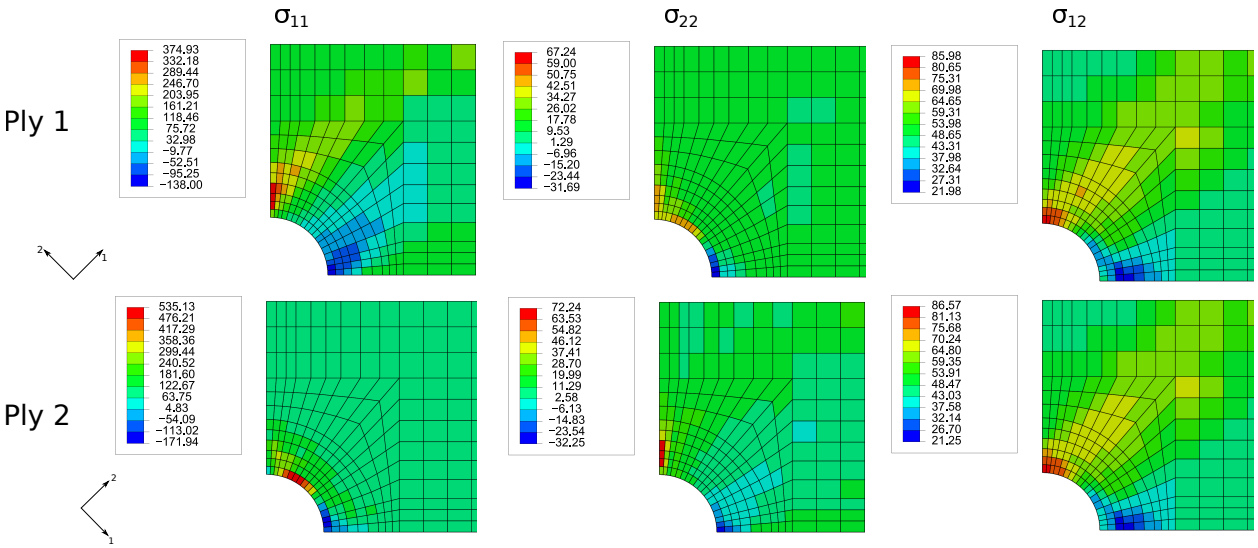

Fig. 19 Stress contour plots for the individual ply in the material coordinate system for 1D-1D model (All units in MPa)

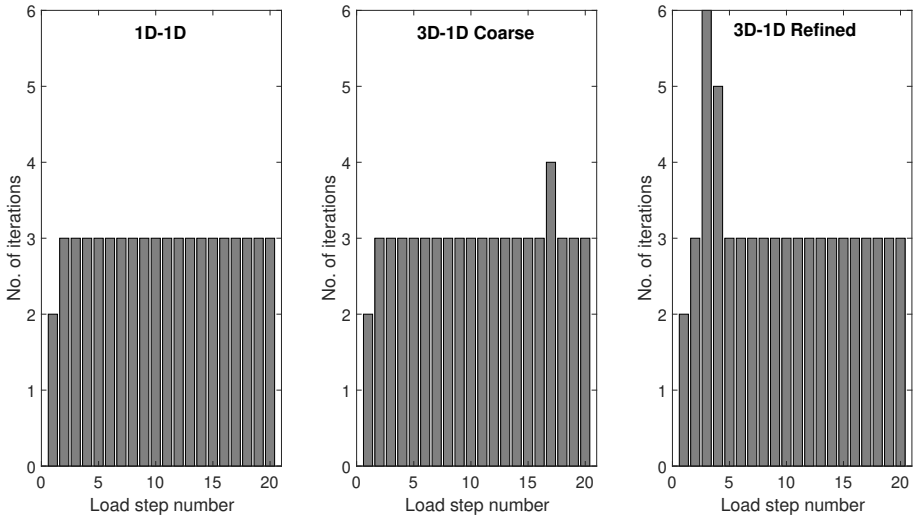

Fig. 20 Convergence behavior of multiscale models for the open-hole specimen under tension

VII. Acknowledgment

This research work has been carried out within the project FULLCOMP (FULLy analysis, design, manufacturing, and health monitoring of COMPosite structures), funded by the European Union Horizon 2020 Research and Innovation program under the Marie Skłodowska-Curie grant agreement No. 642121. Authors would also like to acknowledge the computational resources provided by HPC@POLITO (http://hpc.polito.it).

References

[1] Liu, X., Furrer, D., Kosters, J., and Holmes, J., "Vision 2040: A Roadmap for Integrated, Multiscale Modeling and Simulation of Materials and Systems," NASA Glenn Research Center, 2018.

[2] Aboudi, J., Arnold, S., and Bednarcyk, B., *Micromechanics of Composite Materials*, Elsevier Inc., 2012. doi:10.1016/C2011-0-05224-9.

[3] Herakovich, C. T., *Mechanics of Fibrous Composites*, Wiley and Sons Ltd., 1997. doi:10.1016/C2011-0-05224-9.

[4] Hashin, Z., and Rosen, B. W., "The Elastic Moduli of Fiber-Reinforced Materials," *Journal of Applied Mechanics*, Vol. 31, No. 2, 1963, pp. 223 – 232. doi:https://doi.org/10.1115/1.3629590, URL http://www.sciencedirect.com/science/article/pii/0001616073900643.

[5] Mori, T., and Tanaka, K., "Average stress in matrix and average elastic energy of materials with misfitting inclusions," *Acta Metallurgica*, Vol. 21, No. 5, 1973, pp. 571 – 574. doi:https://doi.org/10.1016/0001-6160(73)90064-3, URL http://www.sciencedirect.com/science/article/pii/0001616073900643.

[6] Huang, Y., Hu, K., Wei, X., and Chandra, A., "A generalized self-consistent mechanics method for composite materials with multiphase inclusions," *Journal of the Mechanics and Physics of Solids*, Vol. 42, No. 3, 1994, pp. 491 – 504. doi:https://doi.org/10.1016/0022-5096(94)90028-0, URL http://www.sciencedirect.com/science/article/pii/0022509694900280.

[7] Segurado, J., Llorca, J., and González, C., "On the accuracy of mean-field approaches to simulate the plastic deformation of composites," *Scripta Materialia*, Vol. 46, No. 7, 2002, pp. 525 – 529. doi:https://doi.org/10.1016/S1359-6462(02)00027-1, URL http://www.sciencedirect.com/science/article/pii/S1359646202000271.

[8] Zhang, D., and Waas, A. M., "A micromechanics based multiscale model for nonlinear composites," *Acta Mechanica*, Vol. 225, No. 4, 2014, pp. 1391–1417. doi:10.1007/s00707-013-1057-1, URL https://doi.org/10.1007/s00707-013-1057-1.

[9] Patel, D., and Waas, A., "Damage and failure modelling of hybrid three-dimensional textile composites: a mesh objective multi-scale approach," *Philosophical Transactions of The Royal Society A-Mathematical Physical And Engineering Sciences*, Vol. 374, No. 2071, 2017. doi:10.1098/rsta.2016.0036.

[10] Zhang, D., Patel, D. K., and Waas, A. M., "A novel two-scale progressive failure analysis method for laminated fiber-reinforced composites," *56th AIAA/ASCE/AHS/ASC Structures, Structural Dynamics, and Materials Conference*, , No. January, 2015, pp. 1–19. doi:10.2514/6.2015-0969.

[11] Zhang, D., Waas, A. M., and Yen, C. F., "Progressive damage and failure response of hybrid 3D textile composites subjected to flexural loading, part II: Mechanics based multiscale computational modeling of progressive damage and failure," *International Journal of Solids and Structures*, Vol. 75-76, 2015, pp. 321–335. doi:10.1016/j.ijsolstr.2015.06.033, URL http://dx.doi.org/10.1016/j.ijsolstr.2015.06.033.

[12] e-Xstream Engineering, "DIGIMAT Software," Louvain-la-Neuve, Belgium, 2018.

[13] Paley, M., and Aboudi, J., "Micromechanical analysis of composites by the generalized cells model," *Mechanics of Materials*, Vol. 14, No. 2, 1992, pp. 127 – 139. doi:https://doi.org/10.1016/0167-6636(92)90010-B, URL http://www.sciencedirect.com/science/article/pii/016766369290010B.

[14] Aboudi, J., Pindera, M.-J., and Arnold, S., "Higher-order theory for functionally graded materials," *Composites Part B: Engineering*, Vol. 30, No. 8, 1999, pp. 777 – 832. doi:https://doi.org/10.1016/S1359-8368(99)00053-0, URL http://www.sciencedirect.com/science/article/pii/S1359836899000530.

[15] Pineda, E. J., Waas, A. M., Bednarcyk, B. A., Collier, C. S., and Yarrington, P. W., "Progressive damage and failure modeling in notched laminated fiber reinforced composites," *International Journal of Fracture*, Vol. 158, No. 2, 2009, pp. 125–143. doi:10.1007/s10704-009-9370-3.

[16] Naghipour, P., Arnold, S. M., Pineda, E. J., Stier, B., Hansen, L., Bednarcyk, B. A., and Waas, A. M., "Multiscale static analysis of notched and unnotched laminates using the generalized method of cells," *Journal of Composite Materials*, Vol. 51, No. 10, 2017, pp. 1433–1454. doi:10.1177/0021998316651708.

[17] Haj-Ali, R., and Aboudi, J., "Nonlinear micromechanical formulation of the high fidelity generalized method of cells," *International Journal of Solids and Structures*, Vol. 46, No. 13, 2009, pp. 2577–2592. doi:10.1016/j.ijsolstr.2009.02.004, URL http://dx.doi.org/10.1016/j.ijsolstr.2009.02.004.

[18] Ricks, T. M., Lacy, T. E., Pineda, E. J., Bednarcyk, B. A., and Arnold, S. M., "Computationally efficient High-Fidelity Generalized Method of Cells micromechanics via order-reduction techniques," *Composite Structures*, Vol. 156, 2016, pp. 2–9. doi:10.1016/j.compstruct.2016.05.093, URL http://dx.doi.org/10.1016/j.compstruct.2016.05.093.

[19] Feyel, F., "Multiscale FE^2 elastoviscoplastic analysis of composite structures," *Computational Materials Science*, Vol. 16, No. 1, 1999, pp. 344 – 354. doi:https://doi.org/10.1016/S0927-0256(99)00077-4, URL http://www.sciencedirect.com/science/article/pii/S0927025699000774.

[20] Meyer, P., and Waas, A. M., "Mesh-objective two-scale finite element analysis of damage and failure in ceramic matrix composites," *Integrating Materials and Manufacturing Innovation*, Vol. 4, No. 1, 2015, p. 18. doi:10.1186/s40192-015-0034-z, URL http://www.immijournal.com/content/4/1/5.

[21] Tikarrouchine, E., Chatzigeorgiou, G., Praud, F., Piotrowski, B., Chemisky, Y., and Meraghni, F., "Three-dimensional FE^2 method for the simulation of non-linear, rate-dependent response of composite structures," *Composite Structures*, Vol. 193, 2018, pp. 165–179. URL https://doi.org/10.1016/j.compstruct.2018.03.072.

[22] Verhoosel, C. V., Remmers, J. J. C., Gutiérrez, M. A., and de Borst, R., "Computational homogenization for adhesive and cohesive failure in quasi-brittle solids," *International Journal for Numerical Methods in Engineering*, Vol. 83, No. 8-9, 2010, pp. 1155–1179. doi:10.1002/nme.2854, URL https://onlinelibrary.wiley.com/doi/abs/10.1002/nme.2854.

[23] Feyel, F., and Chaboche, J. L., "FE2 multiscale approach for modelling the elastoviscoplastic behaviour of long fibre SiC/Ti composite materials," *Computer Methods in Applied Mechanics and Engineering*, Vol. 183, No. 3, 2000, pp. 309 – 330. doi:https://doi.org/10.1016/S0045-7825(99)00224-8, URL http://www.sciencedirect.com/science/article/pii/S0045782599002248.

[24] Chinesta, F., Ammar, A., and Cueto, E., "Recent Advances and New Challenges in the Use of the Proper Generalized Decomposition for Solving Multidimensional Models," *Archives of Computational Methods in Engineering*, Vol. 17, No. 4, 2010, pp. 327–350. doi:10.1007/s11831-010-9049-y, URL https://doi.org/10.1007/s11831-010-9049-y.

[25] Néron, D., and Ladevèze, P., "Proper Generalized Decomposition for Multiscale and Multiphysics Problems," *Archives of Computational Methods in Engineering*, Vol. 17, No. 4, 2010, pp. 351–372. doi:10.1007/s11831-010-9053-2, URL https://doi.org/10.1007/s11831-010-9053-2.

[26] Radermacher, A., Bednarcyk, B., Stier, B., Simon, J., Zhou, L., and Reese, S., "Displacement-based multiscale modeling of fiber-reinforced composites by means of proper orthogonal decomposition," *Advanced Modeling and Simulation in Engineering Sciences*, Vol. 3, No. 1, 2016, p. 29. doi:10.1186/s40323-016-0082-8, URL https://doi.org/10.1186/s40323-016-0082-8.

[27] Kanouté, P., Boso, D. P., Chaboche, J. L., and Schrefler, B. A., "Multiscale Methods for Composites: A Review," *Archives of Computational Methods in Engineering*, Vol. 16, No. 1, 2009, pp. 31–75. doi:10.1007/s11831-008-9028-8, URL https://doi.org/10.1007/s11831-008-9028-8.

[28] Carrera, E., Cinefra, M., Zappino, E., and Petrolo, M., *Finite Element Analysis of Structures Through Unified Formulation*, Wiley and Sons Ltd., 2014. doi:10.1002/9781118536643.

[29] Kaleel, I., Petrolo, M., Waas, A. M., and Carrera, E., "Micromechanical Progressive Failure Analysis of Fiber- Reinforced Composite Using Refined Beam Models," *Journal of Applied Mechanics*, Vol. 85, No. February, 2018, pp. 1–8. doi:10.1115/1.4038610.

[30] Pagani, A., and Carrera, E., "Large-deflection and post-buckling analyses of laminated composite beams by Carrera Unified Formulation," *Composite Structures*, Vol. 170, 2017, pp. 40–52. doi:10.1016/j.compstruct.2017.03.008, URL http://linkinghub.elsevier.com/retrieve/pii/S0263822317306499.

[31] Carrera, E., Guarnera, D., and Pagani, A., "Static and free-vibration analyses of dental prosthesis and atherosclerotic human artery by refined finite element models," *Biomechanics and Modeling in Mechanobiology*, Vol. 17, No. 2, 2018, pp. 301–317. doi:10.1007/s10237-017-0961-z, URL https://doi.org/10.1007/s10237-017-0961-z.

[32] Petrolo, M., Nagaraj, M., Kaleel, I., and Carrera, E., "A global-local approach for the elastoplastic analysis of compact and thin-walled structures via refined models," *Computers & Structures*, Vol. 206, 2018, pp. 54 – 65. doi:https://doi.org/10.1016/j.compstruc.2018.06.004, URL http://www.sciencedirect.com/science/article/pii/S0045794918301159.

[33] Kaleel, I., Petrolo, M., Waas, A., and Carrera, E., "Computationally efficient, high-fidelity micromechanics framework using refined 1D models," *Composite Structures*, Vol. 181, 2017, pp. 358–367. doi:https://doi.org/10.1016/j.compstruct.2017.08.040, URL http://www.sciencedirect.com/science/article/pii/S0263822317324947.

[34] Miehe, C., "Numerical computation of algorithmic (consistent) tangent moduli in large-strain computational inelasticity," *Computer Methods in Applied Mechanics and Engineering*, Vol. 134, No. 3, 1996, pp. 223 – 240. doi:https://doi.org/10.1016/0045-7825(96)01019-5, URL http://www.sciencedirect.com/science/article/pii/0045782596010195.

[35] Carrera, E., and Petrolo, M., "Refined Beam Elements with only Displacement Variables and Plate/Shell Capabilities," *Meccanica*, Vol. 47, 2011, pp. 537–556. doi:10.1007/s11012-011-9466-5.

[36] Carrera, E., Kaleel, I., and Petrolo, M., "Elastoplastic analysis of compact and thin-walled structures using classical and refined beam finite element models," *Mechanics of Advanced Materials and Structures*, In Press. doi:10.1080/15376494.2017.1378780, URL http://dx.doi.org/10.1080/15376494.2017.1378780.

[37] Sun, C., and K.J., Y., "Elastic-Plastic Analysis of AS4/PEEK Composite Laminate Using a One-Parameter Plasticity Model," *Journal of Composite Materials*, Vol. 26, No. 2, 1992, pp. 293–308. doi:10.1177/002199839202600208.

[38] Vogler, M., Rolfes, R., and Camanho, P. P., "Mechanics of Materials Modeling the inelastic deformation and fracture of polymer composites -Part I : Plasticity model," *Mechanics of Materials*, Vol. 59, 2013, pp. 50–64. doi:10.1016/j.mechmat.2012.12.002.

[39] von Mises, R., "Mechanics of solid bodies in the plastically-deformable state," *Mechanik der festen Körper in plastisch-deformablen Zustand*, Vol. 4, 1913, pp. 582–592.

[40] Kouznetsova, V., Brekelmans, W. A. M., and Baaijens, F. P. T., "An approach to micro-macro modeling of heterogeneous materials," *Computational Mechanics*, Vol. 27, No. July 2000, 2001, pp. 37–48. doi:10.1007/s004660000212.

[41] Miehe, C., and Koch, A., "Computational micro-to-macro transitions of discretized microstructures undergoing small strains," *Archive of Applied Mechanics*, Vol. 72, No. 4, 2002, pp. 300–317. doi:10.1007/s00419-002-0212-2.

[42] Geers, M. G., Kouznetsova, V. G., Matouš, K., and Yvonnet, J., *Homogenization Methods and Multiscale Modeling: Nonlinear Problems*, American Cancer Society, 2017, pp. 1–34. doi:10.1002/9781119176817.ecm2107.

[43] Spahn, J., Andrä, H., Kabel, M., and Müller, R., "A multiscale approach for modeling progressive damage of composite materials using fast Fourier transforms," *Computer Methods in Applied Mechanics and Engineering*, Vol. 268, 2014, pp. 871–883. doi:10.1016/j.cma.2013.10.017, URL http://dx.doi.org/10.1016/j.cma.2013.10.017.

[44] Dagum, L., and Menon, R., "OpenMP: An Industry-Standard API for Shared-Memory Programming," *IEEE Comput. Sci. Eng.*, Vol. 5, No. 1, 1998, pp. 46–55. doi:10.1109/99.660313, URL https://doi.org/10.1109/99.660313.

[45] O' Higgins, R., "An experimental and numerical study of damage initiation and growth in high strength glass and carbon fiber-reinforced composite materials," Ph.D. thesis, University of Limerick, 2007.

[46] O' Higgins, R., McCarthy, C. T., and McCarthy, M. A., "Effects of Shear- Transverse Coupling and Plasticity in the Formulation of an Elementary Ply Composites Damage Model, Part I: Model Formulation and Validation," *Strain*, Vol. 48, No. 1, 2012, pp. 49–58. doi:10.1111/j.1475-1305.2010.00797.x.

[47] Kaleel, I., Petrolo, M., and Carrera, E., "Elastoplastic and progressive failure analysis of fiber-reinforced composites via an efficient nonlinear microscale model," *Aerotecnica Missili and Spazio*, Vol. 97, No. 2, 2018, pp. 103–110. doi:10.1007/BF03405805.